# Electron beam quality in a cyclotron autoresonance accelerator

B. Hafizi,[1] P. Sprangle,[2] and J. L. Hirshfield[3]
[1]*Icarus Research, Post Office Box 30780, Bethesda, Maryland 20824-0780*
[2]*Beam Physics Branch, Plasma Physics Division, Naval Research Laboratory, Washington, D.C. 20375*
[3]*Omega-P, Inc., 2008 Yale Station, New Haven, Connecticut 06520*
*and Yale University, Post Office Box 6666, New Haven, Connecticut 06511*
(Received 2 May 1994)

An analysis of the electron beam dynamics in a cyclotron autoresonance accelerator (CARA) is presented. The beam is to be employed in harmonic convertor experiments to generate high-power centimeter-wavelength microwaves, with potential application as a driver for a next-generation electron-positron collider. The presentation will highlight the quality of the electron beam generated by this acceleration mechanism. For beam energies up to about 1 MeV and beam currents up to 50 A, the evolution of the axial velocity spread is determined by a self-consistent numerical solution of the governing nonlinear equations for an ensemble of electrons with finite initial emittance. It is shown that the requirement for an up-tapered guide magnetic field to maintain resonance leads to a diminution of the axial velocity (due to the mirror effect) that eventually causes the acceleration to cease. It is also shown that under some conditions a CARA can have an acceleration efficiency approaching 100%. An estimate is given, and examples are considered for the deterioration of a CARA beam's spatiotemporal character arising from self-fields.

PACS number(s): 41.75.Ht, 29.17.+w, 29.27.Fh

## I. INTRODUCTION

The cyclotron autoresonant accelerator (CARA) may have application as a compact, low-energy injector for a high-gradient accelerator or for use in a source of radiation that requires moderate-energy gyrating electrons. Recent calculations of the efficiency for production of radio-frequency (rf) power at a harmonic of the rotation frequency for an electron beam prepared using a CARA show that good beam quality is important for achieving high efficiency [1]. For example, when a nonlinear (resonant) taper in a magnetic field is employed in the harmonic converter, fifth harmonic conversion efficiency at 14.28 GHz was predicted to fall from 60% to 40% when the axial velocity spread was increased from zero to 6% in a 10 A, 400 kV electron beam. It is thus crucial to understand the origins of finite velocity spread during cyclotron autoresonant acceleration in order to design accelerators capable of producing beams with spreads below 1%. This paper presents the results of an analytical and numerical study of the limits on achievable energy, and also the evolution of the axial velocity spread during acceleration by a CARA operating in the $TE_{11}$ mode at $S$ band.

Prior theoretical studies of the acceleration process [2,3] have shown that rapid trapping of particles occurs at the resonant phase [4,5], that substantial energy gain can be obtained [6,7], but that a practical upper limit to beam energy will exist when a fast-wave rf accelerating field and an uptapered guide magnetic field is employed [8–10]. If an accelerating field with a phase velocity equal exactly to the light velocity is employed, then—in principle—unlimited acceleration can occur. Means for arranging this in practice include the use of dielectrically-lined waveguides or coaxial waveguides operating in the TEM mode. For the former, acceleration gradients determined in our analysis to date have been smaller than those for fast-wave unlined waveguides, and orbiting particles are not prevented from intersecting the inner wall at a relatively low energy. For the latter, elementary considerations show that axicentric orbits experience acceleration to an energy no greater than the potential drop between the inner and outer conductors. For properly phased electrons with fixed, small off-axis displacement of guiding centers, the energy increases with time like $t^{2/5}$ in the asymptotic limit. This is to be compared with the $t^{2/3}$ scaling for the conventional autoresonance acceleration. As a result, consideration here will be limited to fast-wave accelerators for producing 10–100 MW beams in the energy range up to several MeV. Such beams are being tested for use in the harmonic generation of centimeter-wavelength radiation to drive a next-generation electron-positron collider or for millimeter-wavelength radiation for tokamak plasma heating [11].

It has been shown by Friedland that cyclotron autoresonance acceleration can occur even when the guide magnetic field taper is not everywhere "resonant," so long as the excursions about the resonant phase are sufficiently small [12]. He makes the valid point that removing the requirements on the magnetic field taper or the guided wave phase velocity for a precise resonance may make simpler the construction of the CARA. This point has been appreciated in other gyroresonance interactions, such as harmonic generation [1], where resonant and nonresonant magnetic tapers have been studied. Friedland considers an accelerator with a uniform guide magnetic field but with an increasing waveguide radius to

 

provide nearly resonant matching along the accelerator. Use of a uniform magnetic field eliminates the axial deceleration due to mirroring, but as a result of the increasing waveguide radius one finds continuously decreasing acceleration gradients. Thus a longer system length would be required to achieve a given energy gain as compared to the tapered magnetic field case.

In the work to be presented here, uniform waveguides are considered with up-tapered magnetic fields that maintain resonance all along the acceleration path. System lengths are on the order of 1 m for energy gains of about 1 MeV for the parameters chosen here for illustration. This acceleration gradient is still about an order of magnitude lower than that found in conventional linear accelerators (LINACS), but the beam produced in a CARA is continuous, with a macropulse current comparable to the peak current in the microbunches of a LINAC beam. To characterize the beam from a CARA, we present results from detailed simulation of the acceleration process to illustrate the quality of the electron beam generated, as measured by the development of the axial velocity spread on the beam. The major simplifying assumption in the simulation is the neglect of self-fields of the beam during the acceleration process. However, estimates of the effect of self-field forces on the spatiotemporal character of the beam after extraction from the accelerator are given. A schematic of one version of a CARA is shown in Fig. 1 [11].

## II. FORMULATION

The Vlasov-Maxwell system of equations is the natural basis for the description of the wave-particle interaction in the CARA. The electrons are injected into the fields of a $TE_{11}$ mode circular waveguide in a tapered, static magnetic field. Beam loading will be accounted for by invoking energy conservation to self-consistently reduce the rf fields as the beam energy increases. Initial conditions for the electrons can be chosen to simulate finite emittance at the entrance to the waveguide. To implement an efficient numerical scheme for the nonlinear analysis of the interaction, it is essential to simplify these equations. This is accomplished by removing the rapidly varying oscillations from the variables that describe the electrons and the electromagnetic field. Self-field effects are neglected.

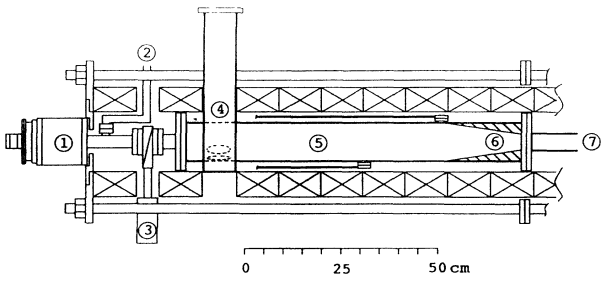


FIG. 1. Schematic of a cyclotron autoresonance accelerator (CARA). 1: Litton electron gun (100 kV, 30 A); 2: vacuum pumping port for electron gun; 3: pneumatic gate valve; 4: input coupler for 2.856 GHz rf; 5: accelerator waveguide; 6: rf absorber; 7: accelerated beam output.

### A. Waveguide field

The rf field in the cylindrical waveguide is a circularly polarized $TE_{11}$ mode whose magnetic and electric components are given by

$$\mathcal{B}_z(\mathbf{r},t)=\mathrm{Re}B_z(z)J_1(k_c r)\exp(-i\omega t+i\phi)\ , \tag{1}$$

$$\mathcal{B}_\perp(\mathbf{r},t)=\mathrm{Re}\frac{1}{k_c^2}\frac{dB_z}{dz}\nabla_\perp J_1(k_c r)\exp(-i\omega t+i\phi)\ , \tag{2}$$

$$\mathcal{E}_\perp(\mathbf{r},t)=\mathrm{Re}\frac{-i\omega}{ck_c^2}B_z(x)\mathbf{e}_z\times\nabla_\perp J_1(k_c r)\exp(-i\omega t+i\phi)\ , \tag{3}$$

where $B_z$ is the spatially varying rf amplitude, $(r,\phi,z)$ denotes cylindrical polar coordinates, $\mathbf{e}_z$ is the unit vector along the $z$ axis, $\omega$ is the frequency, $J_1$ is the ordinary Bessel function of order 1, $k_c=p'_{11}/a$ is the transverse wave number, $a$ is the cavity radius, and $p'_{11}$ is the first zero of $dJ_1(x)/dx$, as is appropriate for the boundary condition on the TE mode. The suffix $\perp$ identifies the component(s) transverse to the $z$ axis, and the gradient operator in the $(r,\phi)$ plane is denoted by $\nabla_\perp$.

In the approximation that the envelope of the rf field varies slowly, it is convenient to express $B_z$ in the quasi-classical form

$$B_z(z)=\hat{B}\exp\left[i\vartheta+ik_z z+i\int_0^z dz'[\Delta\tilde{k}(z')+i\tilde{\Gamma}(z')]\right]\ , \tag{4}$$

where $\vartheta$ is a constant phase, $\hat{B}$ is a constant amplitude, $k_z$ is the axial wave number, and $\Delta\tilde{k}(z)$ and $\tilde{\Gamma}(z)$ are the slowly varying wave number shift and damping rate, respectively. In the absence of a driving current, the latter two quantities vanish and the vacuum dispersion relation obtains $\omega^2/c^2=k_z^2+k_c^2$.

### B. Equations of motion of electrons

The relativistic Lorentz equations of motion of an electron are given by

$$\frac{d\mathbf{p}}{dt}=-|e|[\mathcal{E}+\frac{\mathbf{v}}{c}\times(\mathcal{B}+\mathbf{B}_0)]\ ,$$

where $\mathbf{v}$ is the velocity, $\mathbf{p}=\gamma m\mathbf{v}$ is the momentum, $\gamma=(1-v^2/c^2)^{-1/2}$ is the relativistic factor, $e$ is the charge on an electron, and $\mathbf{B}_0$ is the guide magnetic field. As is usual in problems involving gyromotion about a magnetic field, it is useful to cast the motion of electrons in guiding center coordinates. For simplicity, consider the case where the guiding center of all the incoming electrons lies on the axis and neglect guiding center drifts. The latter approximation is commonly employed in the analysis of the cyclotron autoresonance maser [13] and simplifies the equations of motion significantly. Inserting the expressions for the rf field, Eqs. (1)–(3), into the Lorentz equation, one obtains a large number of terms, many of which vary rapidly, i.e., on the time scale associated with the gyrofrequency. Averaging the equations, one obtains the following set of slowly evolving equations of motion:

$$\frac{dU_\perp}{d\zeta}=\frac{2bJ_1'(k_c\rho)}{\beta_z}\{[1-(n+\Delta k)\beta_z]\cos\psi-\Gamma\beta_z\sin\psi\}\exp\left[-\int_0^\zeta d\zeta'\Gamma(\zeta')\right]+\frac{U_\perp db_0/d\zeta}{2b_0}\ , \tag{5}$$

$$\frac{dU_z}{d\zeta}=2bJ_1'(k_c\rho)\frac{U_\perp}{U_z}[(n+\Delta k)\cos\psi-\Gamma\sin\psi]\exp\left[-\int_0^\zeta d\zeta'\Gamma(\zeta')\right]-\frac{U_\perp^2 db_0/d\zeta}{2U_z b_0}\ , \tag{6}$$

$$\frac{d\psi}{d\zeta}=\Delta+\Delta k-2b\frac{J_1(k_c\rho)}{\beta_z}\left\{\frac{[1-(n+\Delta k)\beta_z]\sin\psi-\Gamma\beta_z\cos\psi}{U_\perp k_c\rho}-\frac{ck_c}{\gamma\omega}\sin\psi\right\}\exp\left[-\int_0^\zeta d\zeta'\Gamma(\zeta')\right]\ , \tag{7}$$

$$\frac{d\Delta}{d\zeta}=\left[\frac{b_0}{U_z}-\frac{n-\Delta}{2}\frac{U_\perp^2}{U_z^2}\right]\frac{db_0/d\zeta}{b_0}-2bJ_1'(k_c\rho)$$
$$\times\{\cos\psi-(n-\Delta)[(n+\Delta k)\cos\psi-\Gamma\sin\psi]\}\frac{U_\perp}{U_z^2}\exp\left[-\int_0^\zeta d\zeta'\Gamma(\zeta')\right]\ , \tag{8}$$

where $U_\perp=p_\perp/mc$, $U_z=p_z/mc$, $\beta_z=U_z/\gamma$, $m$ is the electronic mass, $c$ is the speed of light *in vacuo*, $n=ck_z/\omega$ is the refractive index, $\zeta=\omega z/c$ is the scaled axial distance, $b=|e|\hat{B}/(2mc^2k_c)$ is the normalized rf amplitude, and $J_1'(x)=dJ_1(x)/dx$. In writing these equations, the guide magnetic field has been expressed as

$$\mathbf{B}_0=-\tfrac{1}{2}B_0'(z)(x\mathbf{e}_x+y\mathbf{e}_y)+B_0(z)\mathbf{e}_z\ ,$$

where $\mathbf{e}_{x,y}$ are unit vectors in the $x$ and $y$ directions, respectively, and $B_0'=dB_0/dz$. This form permits the use of guide-field tapering in order to maintain the resonant interaction and hence enhance the efficacy of the acceleration process. Additionally, the $x$ and $y$ coordinates and momenta have been expressed as follows:

$$p_x=p_\perp\cos\theta\ ,$$
$$p_y=p_\perp\sin\theta\ ,$$
$$x=X+\rho\sin\theta\ ,$$
$$y=Y-\rho\cos\theta\ ,$$

where $p_\perp$ is the transverse momentum, $\theta$ is the gyroangle, $\rho=p_\perp/m\Omega_0$ is the gyroradius, $\Omega_0=|e|B_0/mc$ is the nonrelativistic gyrofrequency, and $X$ and $Y$ are the guiding center coordinates, which are assumed to be zero for simplicity. Further, $b_0=\Omega_0/\omega$ is the gyrofrequency normalized to the rf frequency, $\Delta k=c\Delta\tilde{k}/\omega$ and $\Gamma=c\tilde{\Gamma}/\omega$ are the normalized wave number shift and damping rate, and

$$\psi=\vartheta+\theta+k_z z-\omega t+\int_0^z dz'\Delta\tilde{k}(z') \tag{9}$$

is the slowly evolving electron phase relative to the rf phase. In Eq. (7), the term in braces proportional to $(ck_c/\gamma\omega)\sin\psi$ represents the gyrofrequency in the axial component of the rf magnetic field. Finally, the detuning is defined by

$$\Delta=\frac{\Omega_0}{\omega\gamma\beta_z}-\left[\frac{1}{\beta_z}-n\right]\ . \tag{10}$$

The approximation of retaining only the resonant terms, as in Eqs. (5)–(8), is a major simplification of the problem. It is an excellent approximation provided the electrons perform several ($>3$) complete gyro orbits in the interaction region.

### C. rf-field equations

To obtain a closed system of equations, it is necessary to supplement Eqs. (5)–(8) with the equations that determine the self-consistent evolution of the wave number shift and damping rate of the rf wave. To do so, we start by writing the electron distribution function in the waveguide as follows:

$$\mathcal{F}(\mathbf{r},\mathbf{p},t)=\frac{I}{|e|}\int d^2r_{\perp 0}d^3p_0dt_0F(\mathbf{r}_{\perp 0},\mathbf{p}_0,t_0)\delta(\mathbf{r}-\tilde{\mathbf{r}}(\mathbf{r}_{\perp 0},\mathbf{p}_0,t_0,t))\delta(\mathbf{p}-\tilde{\mathbf{p}}(\mathbf{r}_{\perp 0},\mathbf{p}_0,t_0,t))\ , \tag{11}$$

where $I$ is the beam current and $F(\mathbf{r}_{\perp 0},\mathbf{p}_0,t_0)$ is the electron distribution as a function of the initial transverse coordinates, $\mathbf{r}_{\perp 0}$, initial momenta $\mathbf{p}_0$, and the entry time $t_0$, into the waveguide. Equation (11) is a statement of phase space density conservation as electrons stream through the waveguide, following the orbits $\tilde{\mathbf{r}}$ and $\tilde{\mathbf{p}}$, where the tilde indicates that the variable is to be expressed as a function of the initial coordinates and momenta, time $t$, and entry time $t_0$. Making use of Eq. (11) for the electron distribution, the wave equation for $B_z$ takes the form

$$\nabla^2B_z+\frac{\omega^2}{c^2}B_z=-\frac{4\pi}{c}\mathbf{e}_z\cdot(\nabla\times\mathbf{J})\ .$$

In this equation, $\mathbf{J}$ denotes the current density phasor, which is related to the actual current density $\mathcal{J}$, through

$$\mathcal{J}=\mathrm{Re}[\mathbf{J}\exp(-i\omega t)]=-|e|\int d^3p\frac{\mathbf{p}}{\gamma m}\mathcal{F}(\mathbf{r},\mathbf{p},t)\ .$$

Making use of Eq. (4), the wave-number shift and the damping rate are given by

$$\Delta k(\zeta)=\frac{2I}{I_0}\frac{(1-n^2)/nb}{(p_{11}'^2-1)J_1^2(p_{11}')}\exp\left[\int_0^{\zeta}d\zeta'\Gamma(\zeta')\right]\int_0^{2\pi/\omega}\frac{dt_0}{2\pi/\omega}d^2r_{\perp 0}d^3p_0F(\mathbf{r}_{\perp 0},\mathbf{p}_0,t_0)J_1'(k_c\tilde{\rho})\frac{\tilde{U}_\perp}{\tilde{U}_z}\sin\tilde{\psi}\ , \tag{12}$$

$$\Gamma(\zeta)=\frac{2I}{I_0}\frac{(1-n^2)/nb}{(p_{11}'^2-1)J_1^2(p_{11}')}\exp\left[\int_0^{\zeta}d\zeta'\Gamma(\zeta')\right]\int_0^{2\pi/\omega}\frac{dt_0}{2\pi/\omega}d^2r_{\perp 0}d^3p_0F(\mathbf{r}_{\perp 0},\mathbf{p}_0,t_0)J_1'(k_c\tilde{\rho})\frac{\tilde{U}_\perp}{\tilde{U}_z}\cos\tilde{\psi}\ , \tag{13}$$

where $I_0=mc^3/|e|$ is 17kA in Système International (SI) units. It should be remarked that Eqs. (12) and (13) are not to be treated as integral equations. Rather, they are simple formulas expressing the wave number shift and growth rate in terms of known variables on the right-hand side. This is readily implemented numerically.

## III. NUMERICAL RESULTS

The simulation results presented here are obtained by following the motion of, typically, a group of 100 electrons in the field of a $TE_{11}$ mode in a circular waveguide, which is immersed in a guide magnetic field. The amplitude of the rf field is assumed to vary slowly due to beam loading of the circuit. The guide field is tapered along the $z$ axis in order to maintain resonance, i.e., $\Omega_0/\gamma=\omega(1-n\beta_z)$ for the average electron. The equations of motion for the electrons, Eqs. (5)–(8), are integrated by a fourth order Runge-Kutta method using $10^4$ mesh points, while $\Delta k(z)$, the wave number shift, and $\Gamma(z)$, the damping rate, are determined explicitly from Eqs. (12) and (13). Energy conservation is used to monitor numerical accuracy. The electrons enter the waveguide as a pencil beam consisting of axicentric orbits but with finite emittance.

The parameters for the first set of simulation results are shown in Table I. Equations (5)–(8), (12), and (13) are general and permit simulation of any desirable initial electron distribution $F(\mathbf{r}_{\perp 0},\mathbf{p}_0,t_0)$. In the present studies, the electron beam is chosen to be monoenergetic but with finite emittance. Nonzero beam emittance implies both a beam radius and a spread in the transverse velocity of the electrons. For an electron current $I$ drawn from a thermionic cathode at temperature $T_c$, the ideal (neglecting space-charge contributions) emittance is given by [14]

$$\epsilon_{\rm th}=\left[\frac{I}{\pi J_c}\right]^{1/2}\left[\frac{T_c}{mc^2}\right]^{1/2},$$

where $J_c$ is the current density at the cathode. The initial emittance value of 14.14 mm mrad in Table I is twice this ideal emittance for a 50-A beam drawn from a 5-cm$^2$ thermionic cathode at a temperature of 0.16 eV. The waveguide radius is chosen to be large enough so that the refractive index is close to unity and, therefore, the interaction is close to autoresonance. As a consequence,

TABLE I. Parameters for simulation of CARA at $S$ band. Waveguide radius permits excitation of all TE and TM modes through $TM_{21}$.

| | |
|---|---|
| Frequency | 2.856 GHz |
| Input power | 50 MW |
| Current | 50 A |
| Waveguide radius | 8.824 cm |
| Refractive index | 0.9373 |
| Initial energy | 100 keV |
| Final energy | 1 MeV |
| Initial normalized emittance | 14.14 mm mrad |
| Initial beam radius | 0.6375 mm |
| Initial rms axial velocity spread | 0.02% |
| Initial magnetic field | 0.593 kG |

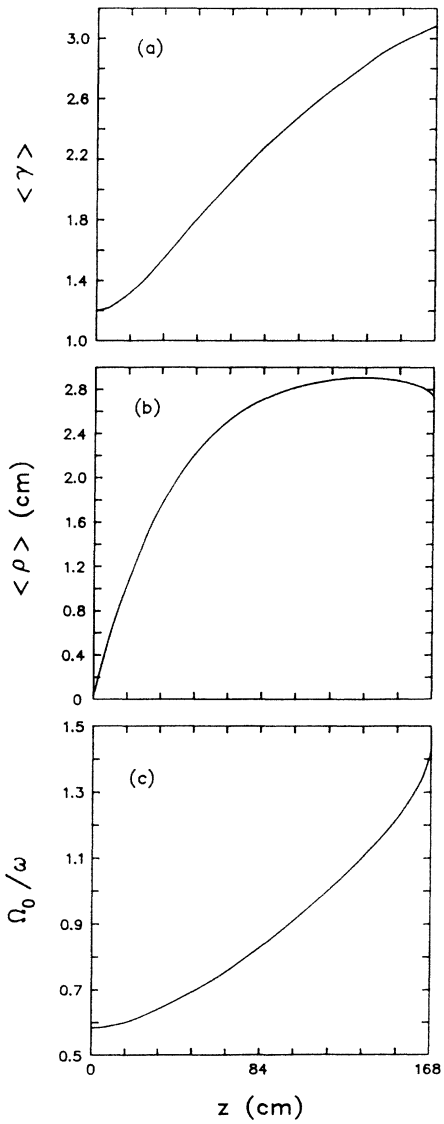


FIG. 2. Results from numerical simulation of CARA operating at the $S$ band with a 8.824-cm waveguide radius. (a) Mean beam relativistic factor; $\langle\ \rangle$ indicates an average over the electron distribution. (b) Mean beam gyroradius. (c) Ratio of gyrofrequency to rf frequency. Abscissa is distance along waveguide.

the waveguide is somewhat overmoded and supports all TE and TM modes through $TM_{21}$.

Figures 2(a), 2(b), and 2(c) show the mean $\gamma$, the mean gyroradius $\rho=\gamma v_\perp/\Omega_0$, where $v_\perp$ is the transverse component of the electron velocity, and the ratio of the gyrofrequency to the rf frequency $\Omega_0/\omega$, all as functions of axial distance $z$. (In the figures, $\langle\ \rangle$ indicates the average over the electron distribution.) Figure 2(a) shows that the beam energy increases to about 1 MeV in a distance of 168 cm. Beyond $\sim$100 cm, the rise in energy is principally directed into the transverse component of the electron velocity. To maintain resonance, this is accompanied by a rise in the magnetic field, which tends to reduce the axial electron velocity due to the transverse components of the magnetic field. This, in turn, leads to a further rise in the field to preserve the resonance. The net effect is the rapid rise observed in Fig. 2(c) and is responsible for restraining the gyroradius from approaching the waveguide radius, as indicted in Fig. 2(b). It is this fortuitous effect that allows one to employ a waveguide with a relatively small radius and enhance the accelerating field for a given input power.

Figure 3(a) shows the increase in the mean beam $\alpha\equiv v_\perp/v_z$ as the electrons are accelerated. The acceleration process, of course, leads to depletion of the rf power down the waveguide, as shown in Fig. 3(b). Finally, the root-mean-square (rms) spread in the axial velocity of the electrons, normalized to the mean axial velocity, is shown in Fig. 3(c). It is observed that the spread in the axial ve-

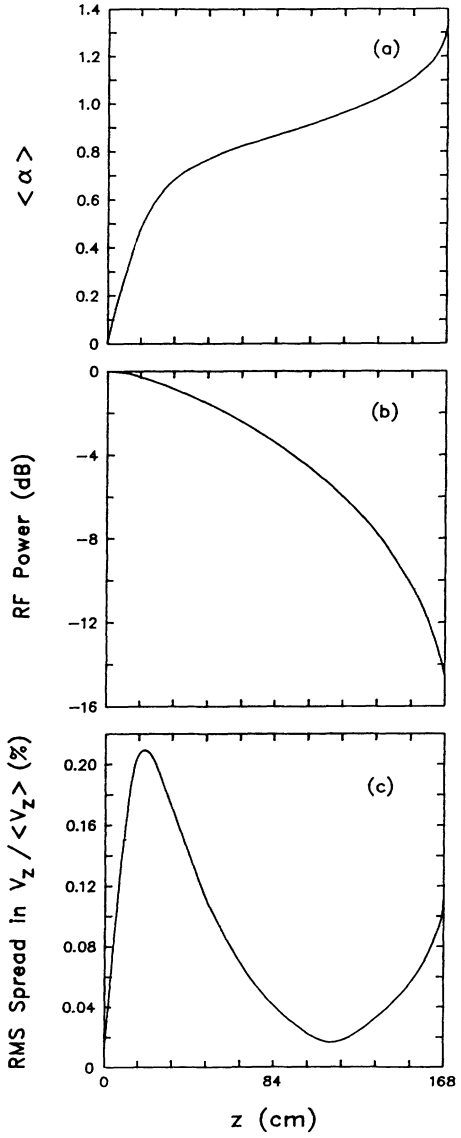


FIG. 3. Results from numerical simulation of CARA operating at the $S$ band with a 8.824-cm waveguide radius. (a) Mean beam $\alpha$. (b) Depletion of rf power. (c) Ratio of root-mean-square spread in axial velocity to mean axial velocity. Abscissa is distance along waveguide.

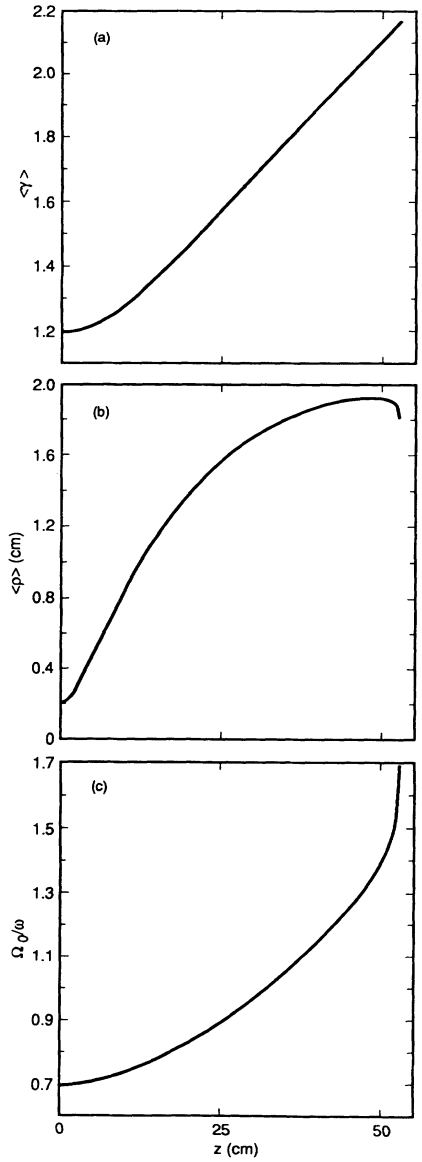


FIG. 4. Results from numerical simulation of CARA operating at the $S$ band with a 4.8-cm waveguide radius. (a) Mean beam relativistic factor; $\langle\ \rangle$ indicates an average over the electron distribution. (b) Mean beam gyroradius. (c) Ratio of gyrofrequency to rf frequency. Abscissa is distance along waveguide.

locity, which is the key figure of merit in evaluating the quality of the beam for radiation generation purposes, is much smaller than 1%. In this example the normalized wavenumber shift $\Delta k$ increases monotonically to $\approx 0.0021$ at $z = 168$ cm.

In a second example, shown in Figs. 4 and 5, a smaller waveguide radius and smaller input power are assumed, compared with the first example; see Table II. The refractive index is smaller, so that acceleration to a lower ultimate energy (0.6 MeV) is found. This waveguide is cutoff to all but the $TE_{11}$ and $TM_{01}$ modes and thus could be more straightforward to excite than that in the first example. An initial axial velocity spread of 1% is assumed; this is seen to grow to $\approx 2\%$ at $z = 38$ cm ($\approx 450$ kV) and to $\approx 3\%$ at $z = 44$ cm ($\approx 500$ kV). These values are the

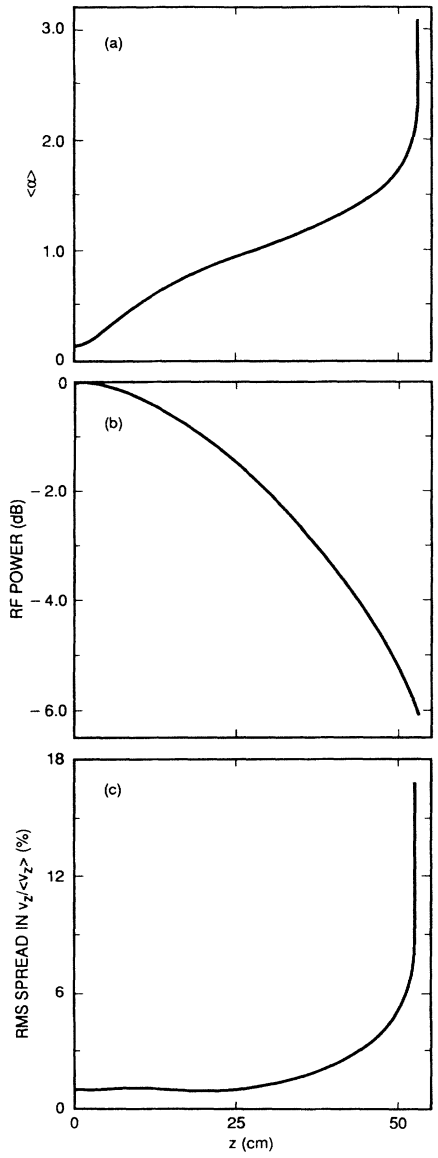


FIG. 5. Results from numerical simulation of CARA operating at the $S$ band with a 4.8-cm waveguide radius. (a) Mean beam $\alpha$. (b) Depletion of rf power. (c) Ratio of root-mean-square spread in axial velocity to mean axial velocity. Abscissa is the distance along the waveguide.

TABLE II. Parameters for simulation of CARA at the $S$ band. Waveguide cutoff to all but $TE_{11}$ and $TM_{01}$ modes.

| | |
|---|---|
| Frequency | 2.856 GHz |
| Input power | 20 MW |
| Current | 30 A |
| Waveguide radius | 4.8 cm |
| Refractive index | 0.7677 |
| Initial energy | 100 keV |
| Final energy | 0.6 MeV |
| Initial normalized emittance | 10.95 mm mrad |
| Initial beam radius | 3.7 mm |
| Initial rms axial velocity spread | 1% |
| Initial magnetic field | 0.7064 kG |

limits of what may be acceptable for some of the applications for such a beam, as discussed in the Introduction. It thus could be that some form of beam conditioning might be required to produce beams of higher quality; means for arranging beam conditioning for a phase-ordered gyrating beam are currently under development. In this example the normalized wavenumber shift $\Delta k$ decreases monotonically to $\approx -0.017$ at the end of the accelerator.

Previous work has discussed acceleration to much higher energies than 1 MeV using this mechanism [6–9]. This may be illustrated by considering the case with refractive index close to unity, $n = 0.9979$; see Table III. For the $TE_{11}$ mode at 2.856 GHz, this requires a waveguide radius of 48 cm. Taking a (hypothetical) rf drive power level of 2.6 GW gives the results shown in Figs. 6 and 7. Here it is seen that indeed acceleration to an energy of over 5 MeV can occur in a distance of 6 m, consistent with earlier results. But the greatly overmoded waveguide, the extreme power level required, and the considerable length of this accelerator do not seem to make it a practical alternative to other available means of acceleration in this energy range.

## IV. LIMITATION IN ENERGY

From the examples discussed in Sec. III and from prior work on electron cyclotron autoresonance acceleration, it is apparent that an upper limit exists to the energy one can reach with this acceleration mechanism when $n \neq 1$ and when an uptapered magnetic field is employed. The

TABLE III. Parameters for simulation of CARA at the $S$ band. Large waveguide radius leads to near-unity refractive index.

| | |
|---|---|
| Frequency | 2.856 GHz |
| Input power | 2.6 GW |
| Current | 30 A |
| Waveguide radius | 48 cm |
| Refractive index | 0.9979 |
| Initial energy | 100 keV |
| Final energy | 5 MeV |
| Initial normalized emittance | 10.95 mm mrad |
| Initial beam radius | 4.7 mm |
| Initial rms axial velocity spread | 0.9% |
| Initial magnetic field | 0.553 kG |

origin of this limit can be seen by examination of Eq. (8). It is apparent from Eq. (7) that by tapering the magnetic field to maintain resonance, $\Delta=0$, electrons rapidly coalesce around the (stable) synchronous phase $\psi=0$. With $d\Delta/dz=0$, the required spatial tapering of the guide field is expressible as

$$\frac{dB_0}{dz} \propto \frac{(\omega/c)B_0}{2(\Omega_0/\omega)mcp_z - np_\perp^2} . \tag{14}$$

This quantity can only remain finite if $p_z > n(\omega/\Omega_0)p_\perp^2/(2mc)$. But as the beam spins up and $p_\perp$ increases, $p_z$ decreases due to the familiar mirror effect, which is represented by the last term in Eq. (8), and the denominator in Eq. (14) approaches zero. Eventually, either the magnetic field gradient becomes too large to be sustained by a realistic coil system and the acceleration ceases, or the particles turn around. It is evident that this effect will occur whether or not the refractive index is greater or less than unity, i.e., whether a slow- or fast-wave circuit is employed. For $n=1$, where continuous acceleration can occur without need for a tapered guide magnetic field, this limit does not exist. Nor does the limit exist when a tapered waveguide radius with a uniform magnetic field is employed [12]. But, as discussed earlier, the latter configuration has a small acceleration gradient.

It is interesting to speculate what these considerations imply when the guide field is aligned antiparallel to the

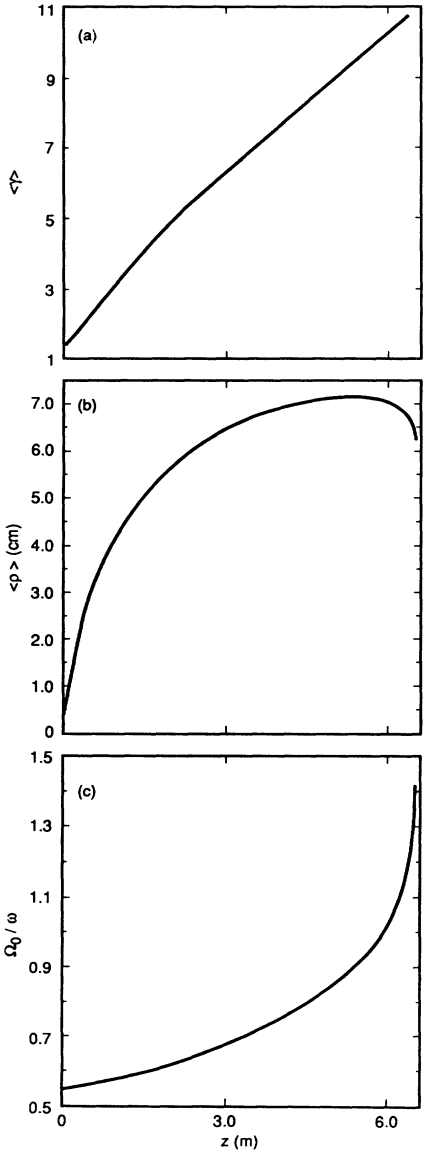


FIG. 6. Results from numerical simulation of CARA operating at the $S$ band with a 48-cm waveguide radius. (a) Mean beam relativistic factor; $\langle\ \rangle$ indicates an average over the electron distribution. (b) Mean beam gyroradius. (c) Ratio of gyrofrequency to rf frequency. Abscissa is distance along waveguide.

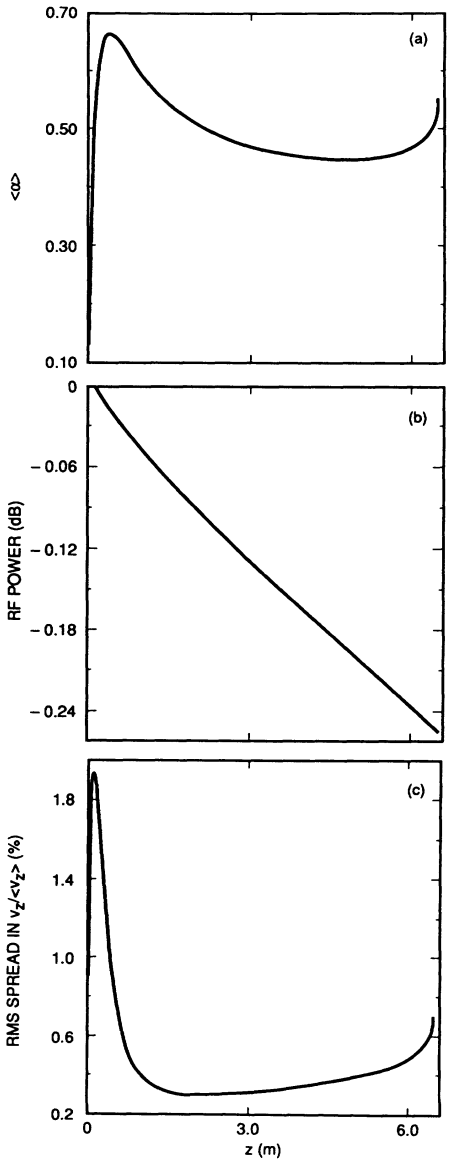


FIG. 7. Results from numerical simulation of CARA operating at the $S$ band with a 48-cm waveguide radius. (a) Mean beam $\alpha$. (b) Depletion of rf power. (c) Ratio of root-mean-square spread in axial velocity to mean axial velocity. Abscissa is distance along waveguide.

direction of wave propagation. If the resonance condition $\Delta=0$ is to be met, one has $n\beta_z=1+|b_0|/\gamma$, which states that resonance occurs when the Doppler shift is large enough to overcome the negative gyrofrequency. In such a case, both the numerator and the denominator in Eq. (14) are negative definite, so that $db_0/dz>0$. Since $b_0$ is negative, this implies that the magnitude of $b_0$ is decreasing along the acceleration path, resulting in an increasing gyroradius. Eventually the particles will hit the wall. It would thus appear that one can avoid a steep guide magnetic field gradient by use of an antiparallel field, but that acceleration will be limited by wall interception, just as in the case for a uniform magnetic field when the guided wave has $n=1$.

In order to gain an idea of the potential of CARA as an accelerator, Fig. 8 summarizes the results of a series of runs for a waveguide of radius 4.8 cm, driven by a 20 MW rf klystron, as a function of beam current. In these runs, for a given current the length of the waveguide is gradually increased until the guide magnetic field begins to rise rapidly. This defines the acceleration length $L$. Figure 8(a) shows that the acceleration length increases with beam current in a nonlinear fashion. On the other hand, the acceleration efficiency, defined by

$$\eta=\frac{(P_b)_f-(P_b)_i}{(P_{\rm rf})_i},$$

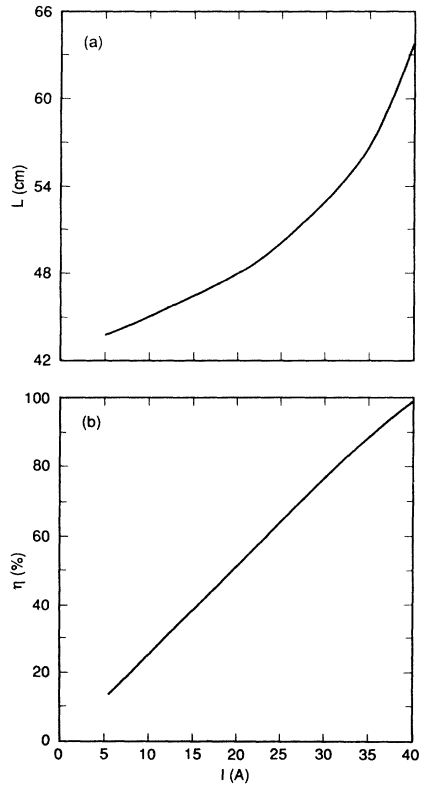


FIG. 8. Results from numerical simulation of CARA operating at the $S$ band with a 4.8-cm waveguide radius, 20 MW initial rf power, and 100 keV initial electron energy. (a) Acceleration length $L$ versus beam current $I$. (b) Acceleration efficiency $\eta$ versus beam current $I$.

is seen to increase almost linearly with current, as shown in Fig. 8(b). In this expression, $P_b$ ($P_{\rm rf}$) denotes the electron beam (rf) power and the suffix $i$ ($f$) refers to the initial (final) value of the quantity. To understand Fig. 8, it must be recalled that in the computations the rf amplitude and wave number (or phase) vary in a self-consistent way, as indicated by Eqs. (12) and (13). These expressions indicate that, to lowest order, the damping and wave number shift are proportional to the current. Thus higher currents lead to faster damping, which implies that a longer acceleration length is required to bring about the same change in the beam power, i.e., lead to the same efficiency. The acceleration length $L$ is seen to rise rapidly for higher currents in Fig. 8(a). Perhaps a more interesting feature of CARA is displayed in Fig. 8(b), which shows that the acceleration efficiency $\eta$ rises with current, reaching up to 100% at 40 A. This may be explained as follows. For low currents where the rf damping is relatively small the beam is rapidly spun up, and due to the mirroring effect the acceleration ceases before significant power is transferred to the electrons. At the higher currents, however, appreciable depletion of rf power occurs, reducing the spin-up rate of the beam. This allows more rf power to be extracted, prior to the termination of the acceleration process due to the mirroring effect.

As a final point regarding the characteristics of CARA, one may ask if this accelerator is, in principle, an adder or a multiplier, i.e., whether it adds a given increment of energy or multiplies the initial energy by a given factor. In order to answer this question in a clear fashion, it is simplest to consider a very low-current and low-emittance beam to avoid unnecessary complications. Two runs were made using, in particular, the same waveguide radius and rf power. In one run, the initial $\gamma$ of 1.2 was increased to 2.25 (in a distance of 43.5 cm). In the other, the initial $\gamma$ of 10.98 was increased to 23.63 (in a distance of 21 m). Based on these two examples, in this energy range one concludes that the CARA is a multiplier and, roughly speaking, a $\gamma$ doubler, subject to availability of rf power.

## V. EFFECT OF BEAM SPACE CHARGE

The analysis and computations presented in this paper neglect self-fields of the beam. Self-fields will cause the spiraling beam to spread along the axial magnetic field and thus to smear out the spatial character of the beam. This could be deleterious for the operation of a harmonic converter utilizing such beams. In this section, an approximate analysis is presented for the rate of spreading along the field lines of a freely drifting helical beam with parameters as prepared by cyclotron autoresonance acceleration. This situation is modeled by considering a segment of the helical beam, initially of minor radius $r_{b0}$, to be a current-carrying uniform cylinder oriented at an angle $\Theta$ with respect to the guide magnetic field. Only motion along the magnetic field is considered. Neglecting wall effects, in the local coordinate system the radial self-electric field $E$ and azimuthal self-magnetic field $B$ at the beam edge are given by

$$E=\frac{-2I}{c\beta r_b} ,$$

$$B=\frac{-2I}{cr_b} ,$$

where $\beta$ is the ratio of the electron speed to $c$, and $r_b$ is the beam radius. We seek an approximate model for the rate of change of $r_b$ as the beam advances in $z$. The $z$ component of the self-force on an edge electron is expressible as

$$F_z=\frac{2I}{I_0}\frac{mc^2}{\beta\gamma^2 r_b}\sin\Theta ,$$

where $I_0$ is defined following Eq. (13) and $\gamma=(1-\beta^2)^{-1/2}$. Since $r_b=z\sin\Theta$ for the edge electron, where the axial displacement $z$ is measured from the instantaneous location of the beam centroid—where no self-field forces act—the expression for the acceleration of an edge electron is

$$\frac{d^2z}{dt^2}=\frac{c^2K}{z} , \tag{15}$$

where $K=2I/(I_0\beta\gamma^3)$; $K/\beta^2$ is the generalized perveance [15], and is typically very small compared to unity. The solution to Eq. (15) is conveniently given by expressing the time as a function of the axial displacement $z$,

$$\frac{ct(z)}{r_{b0}}=\frac{\sqrt{2/K}}{\sin\Theta}W(\ln^{1/2}(z\sin\Theta/r_{b0})) , \tag{16}$$

where $W(x)=\int_0^x dt\exp(t^2)$ is a tabulated function [16].

The effect of self-field forces on the beam equilibrium can be measured by the axial distance $D$ a beam can drift before an edge electron outruns an on-axis electron by a quarter guide wavelength, i.e., $D=c\beta_z t(\pi c/2n\omega)$. Using the helical beam resonance relation, $\tan\Theta=n\beta_\perp/(1-n\beta_z)$ where $\beta_\perp=v_\perp/c$, the drift distance $D$ can be evaluated for the examples presented in Sec. III. For the first example (Table I; 1 MeV, $\alpha=1.3$, $r_{b0}=0.15$ mm) one finds $D=40$ cm, or 3.5 guide wavelengths. For the second example (Table II; 0.6 MeV, $\alpha=1.5$, $r_{b0}=1.75$ mm) one finds $D=48$ cm, or 3.5 guide wavelengths. [In this case, the beam is assumed to be extracted after 45 cm of acceleration in order to avoid the final rapid rise in the velocity spread shown in Fig. 5(c).] For the third example (Table III; 5 MeV, $\alpha=0.55$, $r_{b0}=2.65$ mm) one finds $D=825$ cm, or 78 guide wavelengths. If in the first example the current is reduced to 10 A and the initial beam radius increased to 2 mm one finds $D=143$ cm, or 13 guide wavelengths. From these examples it is seen that the drift distance available before the beam loses its helical character as a result of self-field forces depends sensitively upon the beam current, energy, and minor radius. This could impose limitations on the uses of such beams.

## VI. CONCLUSIONS

The equations of motion have been analyzed for electrons accelerated by the circularly polarized $TE_{11}$ mode of an $S$-band klystron in a cylindrical waveguide with an externally imposed axisymmetric spatially tapered static magnetic field. When the magnetic field is appropriately adjusted, this configuration is known as a cyclotron autoresonance accelerator (CARA) since the particle energy and axial momentum automatically fulfill the resonance condition along the acceleration path—even for nonluminous waves. Under some conditions, it has been shown that nearly complete exchange of microwave power into beam power can occur, so that the CARA can have an acceleration efficiency approaching 100%. The nature of the practical upper energy limit for this acceleration mechanism has been explored, and it has been shown that the requirement in the up-tapered magnetic field eventually leads to a diminution in axial velocity due to the mirror effect and causes the acceleration to cease. By following the trajectories of an ensemble of electrons, injected with finite emittance, the evolution of the axial velocity spread on the beam has been determined. Numerical examples are given in the parameter range appropriate for use of spatiotemporally modulated beams produced in a CARA for harmonic generators to produce multi-MW, cm- and mm-wavelength rf power for future linear colliders and for tokamak plasma heating and control.

The effects of self-fields on the helical nature of beams produced in a CARA have been discussed. Significant orbit spreading due to self-fields has been shown to occur for beams with relatively small minor radius, high current, and low energy. This suggests that a beam conditioning means that to oppose the self-fields could increase the utility of such beams. One possible means of beam conditioning that is currently receiving attention arises from the strong trapping, near resonance phase that occurs in the CARA. The phase focusing forces associated with this trapping could oppose self-field effects, much as in a conventional linear accelerator.

## ACKNOWLEDGMENTS

This work was supported by the Office of Naval Research and the Department of Energy.

[1] J. L. Hirshfield, Phys. Rev. A **46**, 5161 (1992); A. K. Ganguly and J. L. Hirshfield, Phys. Rev. Lett. **70**, 291 (1993).

[2] A. A. Kolomenskii and A. N. Lebedev, Dokl. Akad. Nauk SSSR **145**, 1259 (1962) [Sov. Phys. Dokl. 7, 745 (1963)].

[3] C. S. Roberts and S. J. Buchsbaum, Phys. Rev. **135**, 381 (1964).

[4] P. Sprangle, L. Vlahos, and C. M. Tang, IEEE Trans. Nucl. Sci. **NS-30**, 3177 (1983).

[5] P. Sprangle and L. Vlahos, Phys. Rev. A **33**, 1261 (1986).

[6] R. Shpitalnik, C. Cohen, F. Dothan, and L. Friedland, J. Appl. Phys. **70**, 1101 (1991).
[7] R. Shpitalnik, J. Appl. Phys. **71**, 1583 (1992).
[8] C. Chen, Phys. Fluids B **3**, 2933 (1991).
[9] C. Chen, Phys. Rev. A **46**, 6654 (1992).
[10] R. Pakter, R. S. Schneider, and F. B. Rizzato, Phys. Rev. E **49**, 1594 (1994).
[11] M. A. LaPointe and J. L. Hirshfield, Bull. Am. Phys. Soc. **39**, 1030 (1994).
[12] L. Friedland, Phys. Plasmas **1**, 421 (1994).
[13] A. W. Fliflet, Int. J. Electron. **61**, 1049 (1986).
[14] S. Humphries, *Charged Particle Beams* (Wiley, New York, 1990), Chap. 7.
[15] J. D. Lawson, *The Physics of Charged-Particle Beams* (Oxford University Press, Oxford, England, 1978), Chap. 3.
[16] E. Jahnke and F. Emde, *Tables of Functions* (Dover, New York, 1945), p. 32.